Self-adaptation and viscous selection in concentrated two-dimensional vortex dipoles

D. Sipp, L. Jacquin, Carlo Cosssu

Self-adaptation and viscous selection in concentrated two-dimensional vortex dipoles

Denis Sipp, Laurent Jacquin, and Carlo Cosssu

Citation: Physics of Fluids (1994-present) **12**, 245 (2000); doi: 10.1063/1.870325
View online: http://dx.doi.org/10.1063/1.870325
View Table of Contents: http://scitation.aip.org/content/aip/journal/pof2/12/2?ver=pdfcov
Published by the AIP Publishing

LETTERS

The purpose of this Letters section is to provide rapid dissemination of important new results in the fields regularly covered by Physics of Fluids. Results of extended research should not be presented as a series of letters in place of comprehensive articles. Letters cannot exceed four printed pages in length, including space allowed for title, figures, tables, references and an abstract limited to about 100 words. ***There is a three-month time limit, from date of receipt to acceptance, for processing Letter manuscripts. Authors must also submit a brief statement justifying rapid publication in the Letters section.***

Self-adaptation and viscous selection in concentrated two-dimensional vortex dipoles

Denis Sipp and Laurent Jacquin
ONERA, 29 Av. de la Division Leclerc, BP 72, F-92322 Châtillon Cedex, France

Carlo Cosssu
ONERA, 29 Av. de la Division Leclerc, BP 72, F-92322 Châtillon Cedex, France and LadHyX, CNRS–Ecole Polytechnique, F-91128 Palaiseau Cedex, France

(Received 16 August 1999; accepted 4 November 1999)

In this Letter we deal with 2D direct numerical simulations of concentrated vortex dipoles. We show that various initial dipolar vorticity distributions evolve towards a specific family of dipoles parametrized by the dipole aspect ratio a/b, where a is the radius of the vortices based on the vorticity polar moment in half a plane and b is the separation between the vortex centroids. This convergence is achieved through viscous effects. The considered Reynolds numbers $\mathrm{Re}=\Gamma/\nu$ are $\mathrm{Re}=3000$ and $\mathrm{Re}=15000$. Moreover, all the dipoles of this family are quasi-steady solutions of the Euler equations. Their scatter plots and drift velocities are given for $a/b<0.3$. © *2000 American Institute of Physics.* [S1070-6631(00)02602-7]

Vortex dipoles may be characterized by the dipole aspect ratio a/b, where a is the radius of the vortices based on the vorticity polar moment[1] in half a plane and b is the separation between the vortex centroids. Extensive studies are available for large values of a/b (typically $a/b>0.4$; see Refs. 2,3 and references herein for review). Studies on more concentrated dipoles (small a/b) are less documented. An investigation of this problem has been made by Cantwell and Rott[4] using a heuristic model for the dipole, based on the superposition of two Lamb–Oseen vortices. This approach does not describe the nonlinear self-adaptation of each vortex. Now, Moore and Saffman[5] explained how arbitrary axisymmetric vorticity structures adapt to an external strain field and Ting and Klein[1] showed how viscosity selects particular vorticity profiles. These two mechanisms concur in the dynamics of concentrated viscous vortex dipoles. In this Letter, we analyze these two basic mechanisms by means of 2D direct numerical simulations of various initial dipolar vorticity distributions.

Flow parameters. Let us consider a vorticity distribution $\omega(x,y)$ which is skew-symmetric with respect to the axis $y=0$. The circulation in the upper half plane is $\Gamma=\langle\omega\rangle$ where the brackets denote $\langle f\rangle=\int\int_{y>0} f dx dy$. The position of the upper vortex is characterized by the vorticity centroids:[1] $x_c=\langle x\omega\rangle/\Gamma$ and $y_c=\langle y\omega\rangle/\Gamma$. Three characteristic radii can be defined using polar moments of vorticity:[1] $a_x=[\langle(x-x_c)^2\omega\rangle/\Gamma]^{1/2}$, $a_y=[\langle(y-y_c)^2\omega\rangle/\Gamma]^{1/2}$ and $a=[a_x^2+a_y^2]^{1/2}$. The distance between the two vortices is $b=2y_c$. In a fixed frame, the drift velocity of the dipole is $U=dx_c/dt$. We consider the following nondimensional quantities: the dipole aspect ratio a/b, the vortex aspect ratio $E=a_x/a_y$, the dipole drift velocity $U2\pi b/\Gamma$ and the Reynolds number $\mathrm{Re}=\Gamma/\nu$. For a small dipole aspect ratio a/b, only the time scales based on a (and not those based on b) have to be considered when considering 2D dynamics. They are the viscous time scale $T_\nu=2\pi a^2/\nu$ and the advective time scale $T_a=2\pi a^2/\Gamma$. These time scales are separated for high Reynolds numbers ($T_\nu/T_a=\mathrm{Re}\gg 1$). The present analysis has been developed in the view of performing 3D stability analyses of concentrated dipoles. 3D instabilities[5,6] develop on a time scale based on the separation distance b, $T_a'=2\pi b^2/\Gamma$ where $T_a'\gg T_a$ if a/b is small. So, it is required that $T_\nu\gg T_a'$, i.e., $\mathrm{Re}(a/b)^2\gg 1$, so as to obtain a quasi-steady-Euler solution with respect to T_a'.

Three sets of dipole aspect ratios a_0/b_0 and Reynolds numbers $\mathrm{Re}_0=\Gamma_0/\nu$ are considered (the subscript 0 refers to time $t=0$): case (α) corresponds to $\mathrm{Re}_0=3142$ and $a_0/b_0=0.067$, case (β) to $\mathrm{Re}_0=3142$ and $a_0/b_0=0.134$ and case (γ) to $\mathrm{Re}_0=15708$ and $a_0/b_0=0.134$. The parameters Re_0 and a_0/b_0 are typical of experimental[7] and numerical studies.[8]

Several vorticity profile types have been used to construct the initial dipolar vorticity distributions. The first (L) refers to a Lamb–Oseen vorticity profile, the second (R) is a Rankine vortex and the third (B) corresponds to a solution inspired by the works of Betz and Kaden for the vortex sheet roll-up resulting from an elliptically loaded wing.[9] In the latter case, the vorticity is constant up to a first radius, then decreases as $r^{-1/2}$ up to a second radius where it vanishes. The fourth case (C) consists of a Lamb–Chaplygin

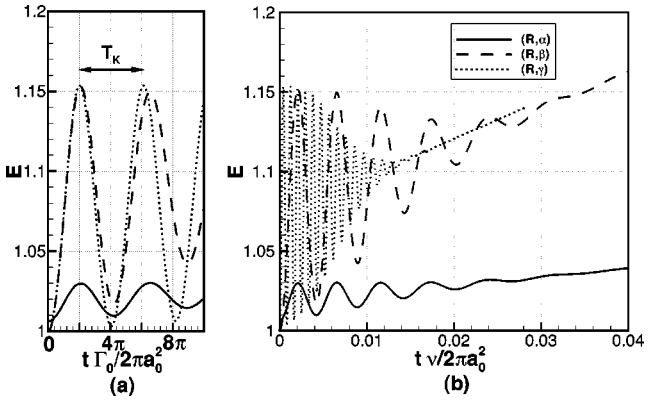

FIG. 1. Vortex aspect ratio E versus (a) time scaled by the advective time; (b) time scaled by the viscous time. Case (R).

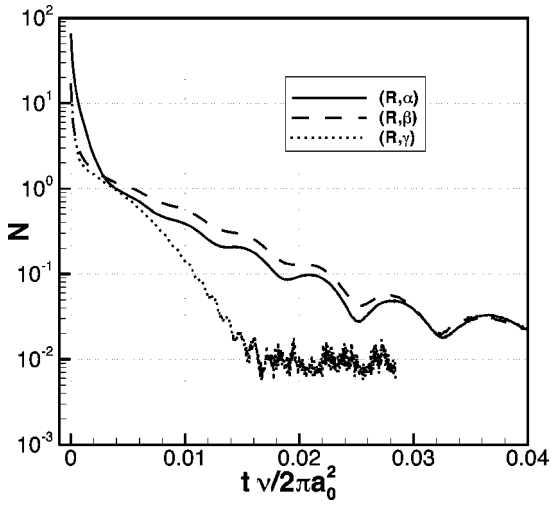

FIG. 2. Euler-residue N versus time scaled by the viscous time. Case (R).

dipole[10,11] whose individual vortices have been moved apart by an arbitrary distance.[8] Within each case (α), (β) and (γ), the constructed initial dipolar vorticity distributions (L,C,B,R) have the same circulation Γ_0, the same radius a_0 and the same separation b_0.

Numerical method. The simulations are performed with a finite-difference code developed at ONERA.[12] The 2D incompressible Navier–Stokes equations are discretized on a rectangular grid. This code is second order both in space and in time. Time integration is achieved using a semi-implicit method (explicit Adams–Bashforth and implicit Crank–Nicolson schemes). The reference frame moves with the dipole at the drift velocity U, so that the dipole position is $x_c = 0$ for all times. We use Dirichlet boundary conditions both for the velocity and the pressure. The velocities at the boundaries are obtained by summing the drift velocity U and the contribution due to the 2D Biot–Savart integral; the pressure is then calculated using the Bernoulli law, the flow being irrotational at large distances. The number of grid cells is, for example, 581 in the x direction and 681 in the y direction for cases (β) and (γ). The corresponding calculation box is $-0.9 \leqslant x/b_0 \leqslant 1.4$ and $-1.7 \leqslant y/b_0 \leqslant 1.7$, which has to be compared to the dipole aspect ratio $a_0/b_0 = 0.134$. A similar grid-resolution is used in case (α). The quality of the simulations is checked by considering the time-evolution of the vortex impulse $\langle y\omega \rangle(t)$, which should exactly be conserved even in viscous situations (see Ref. 1, p. 137): it turns out that the error on this quantity remains less than 0.04% in all simulations. An asymmetric box is used here since the dipoles become slightly asymmetric with respect to $x=0$ because of viscous effects. This asymmetry mainly affects the outer region of the dipoles where the vorticity is very small. In order to conserve precisely $\langle y\omega \rangle(t)$, the computation box must contain the entire vortical zone so that we had to extend it downstream from the dipole.

Evolution versus time. On the time scale T_a, each vortex core is subjected to rapid oscillations due to the nonlinear term of the vorticity equation. This is seen in Fig. 1(a), where we have sketched the vortex aspect ratio E versus the time scaled by the advective time for the Rankine vortex case (R) using the Reynolds numbers and dipole aspect-ratios (α), (β) and (γ) (see above for a definition). This oscillating behavior can be understood by considering for instance the Kirchhoff vortex model, that is a steadily rotating elliptic vortex patch of vorticity ω_0. If the ellipse is close to a circle, its angular velocity is[13] $\Omega = \omega_0/4$. This motion induces an oscillation period of E equal to $T_K \Gamma_0 / 2\pi a_0^2 = 4\pi$. This theoretical value corresponds to the one observed in Fig. 1(a), as expected.

In Fig. 1(b), E is sketched versus the time scaled by the viscous time. The oscillations are subjected to a viscous damping which leads to a quasi-steady solution of the Euler equations. Let us introduce the Euler-residue $N = [\langle (\mathbf{u}$

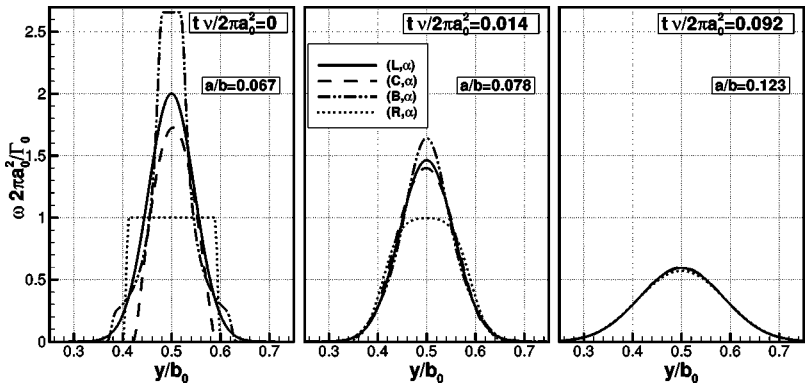

FIG. 3. Evolution of vorticity distributions along a line through the vorticity peaks of the dipoles. Only the domain $0.25 \leqslant y/b_0 \leqslant 0.75$ has been represented. These plots are skew-symmetric with respect to $y/b_0 = 0$. Case (α).

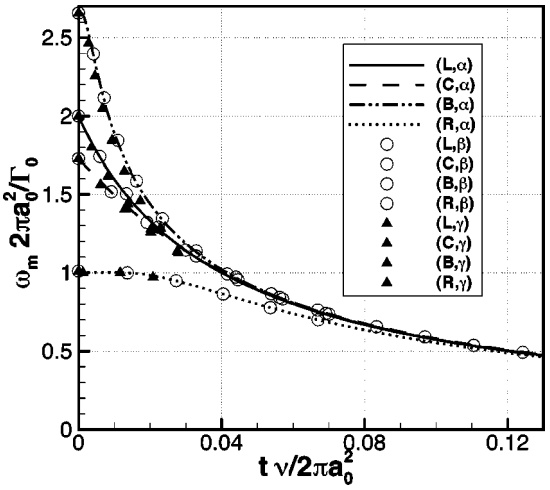

FIG. 4. Peak vorticity ω_m normalized by Γ_0 and a_0 versus time scaled by the viscous time.

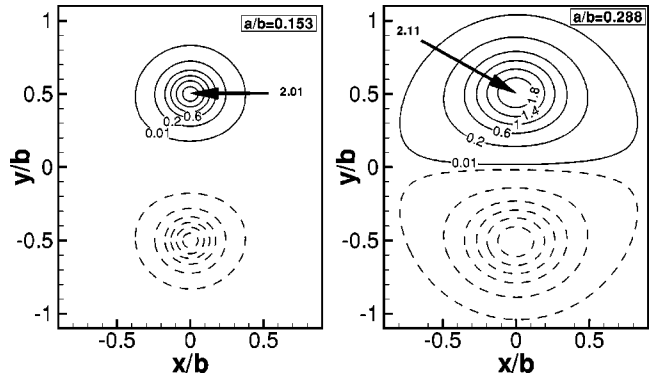

FIG. 6. Vorticity distributions of the dipoles for $a/b=0.153,0.288$. The iso-levels represent the quantity $\omega 2\pi a^2/\Gamma$.

$\cdot \nabla \omega)^2\rangle/\langle \omega^2\rangle]^{1/2}\cdot 2\pi b^2/\Gamma$, which compares the inviscid evolution time scale of the vorticity distribution with the advective time T_a' based on b. As shown in Fig. 2, this quantity which is used to evaluate the steadiness of the flow on the time scale T_a', is subjected to a 3 decade decrease, then it stabilizes. This last phase corresponds to an equilibrium between two antagonistic effects of the viscosity: on the one hand, viscosity damps the oscillations of the type shown in Fig. 1(a) and, on the other hand, it continuously modifies the basic flow.

In Fig. 3, the evolution of the vorticity profiles is shown along a line through the vorticity peaks of the dipoles for the various initial vorticity profile types (L,C,B,R), given a Reynolds number and a dipole aspect ratio [case (α)]. It is seen that all vorticity distributions collapse onto a single one through viscous effects. The time evolution of a/b (not shown here) is the same for all initial vorticity profile types (L,C,B,R). This is due to the fact that only concentrated vorticity distributions are considered here. It can be understood by considering the two following arguments. First, since the vortex impulse $\langle y\omega\rangle(t)$ is constant, the distance between the two centroids $b=2\langle y\omega\rangle/\Gamma$ can only change because of a modification of Γ. For concentrated vorticity distributions, the diffusion of vorticity across the plane $y=0$ is negligible so that Γ and b stay almost constant. Secondly, for an isolated vortex of circulation Γ_0 and of initial core radius a_0, it can be shown [see Eq. (1.2.28b) in Ref. 1] that $a(t)/a_0=(1+4t\nu/a_0^2)^{1/2}$ whatever the initial vorticity profile type. The same law is observed in our simulations. As a consequence, the same time evolution of a/b is obtained for all initial vorticity profile types (L,C,B,R) in each case (α), (β) and (γ). In Fig. 4, we have sketched, for all cases, the evolution of the dipole peak vorticity versus the time scaled by the viscous time. This figure shows, first, that whatever the aspect ratio and Reynolds number, each type of dipole $(L,C,B$ or $R)$ is characterized by a unique curve. Secondly, these four curves converge onto a single one. The conclusion is that the dipoles evolve towards a single structure on the time scale T_ν.

Evolution versus a/b. We now prove that, whatever the initial vorticity profile types (L,C,B,R) and parameters a_0/b_0, Re_0, all flows evolve towards a unique family of dipoles parametrized by a/b. In Fig. 5(a), we have sketched the peak vorticity ω_m normalized with the current Γ and a versus the current dipole aspect ratio a/b for all simulations. A comparison between cases (β) and (γ) shows that the different curves do not depend on the Reynolds number (for

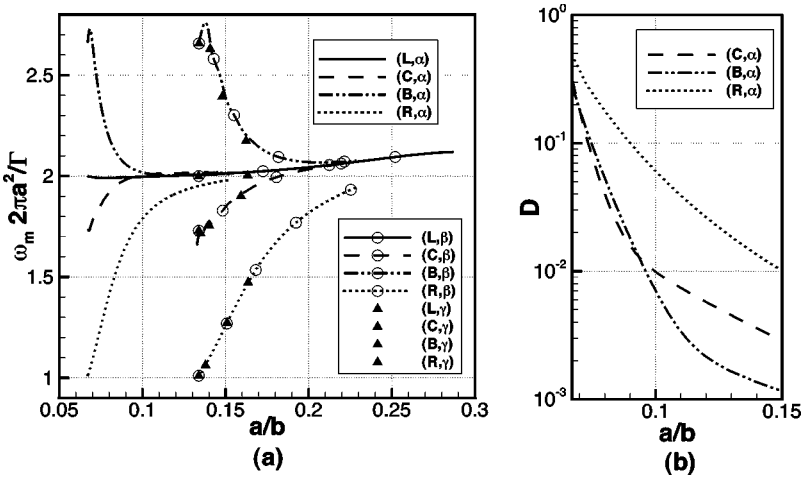

FIG. 5. (a) Peak vorticity ω_m normalized by Γ and a versus the dipole aspect ratio a/b. (b) Deviation D between (C,B,R) simulations and (L) simulation versus a/b.

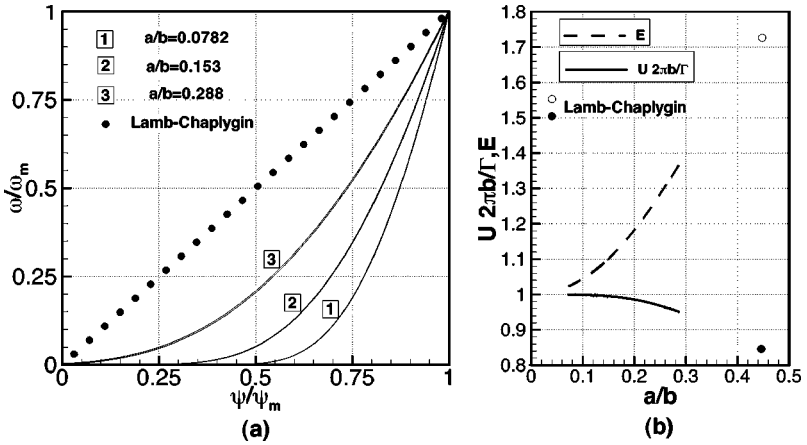

FIG. 7. (a) Scatter plots for the dipoles with $a/b=0.0782,0.153,0.288$. Only the domain $\psi/\psi_m>0$ has been figured since the plots are odd with respect to the origin. (b) Drift velocity $U2\pi b/\Gamma$ and vortex aspect ratio E vs a/b. The circles refer to the Lamb–Chaplygin steady-Euler solution.

the considered Reynolds numbers), so that each curve characterizes an initial vorticity profile. All these curves converge onto a single one, so that a unique family of dipoles parametrized by a/b is obtained. Note that this convergence is achieved with an L_2-norm of the whole vorticity field, i.e., not only the peak vorticity is subjected to convergence, but the whole dipolar vorticity distribution. For example, Fig. 5(b) shows for the simulations of case (α), vs a/b, the deviation $D=[\langle(\omega_I\cdot 2\pi a_I^2/\Gamma_I-\omega_L\cdot 2\pi a_L^2/\Gamma_L)^2\rangle/\langle(\omega_L\cdot 2\pi a_L^2/\Gamma_L)^2\rangle]^{1/2}$ between the vorticity distribution of the (L) simulation (subscript L) and those of the (C,B,R) simulations (subscript $I=C,B,R$). The above family corresponds to dipoles whose normalized peak vorticity $\omega 2\pi a^2/\Gamma$ is close to 2 for $a/b\leqslant 0.3$. Figure 6 shows examples of vorticity distributions belonging to this family. Figure 7(a) gives the scatter plots $\omega/\omega_m=f(\psi/\psi_m)$ for the dipoles corresponding to three different a/b: three lines are obtained, which confirms that the dipoles are quasi-steady solutions of the Euler equations. Figure 7(b) shows the drift velocity $U2\pi b/\Gamma$ and the vortex aspect ratio E versus a/b. The corresponding quantities obtained for the Lamb–Chaplygin steady-Euler solution, for which $a/b=0.4478$, are given for reference.

From the presented results we conclude that various initial dipolar vorticity distributions evolve, through viscous effects, towards a specific family of dipoles parametrized by the dipole aspect ratio a/b. All the dipoles of this family are quasi-steady solutions of the Euler equations and we conjecture that the Lamb–Chaplygin dipole could be a member of this family, even if this is not proved in the present study.

[1] L. Ting and R. Klein, *Viscous Vortical Flows*, Lecture Notes in Physics (Springer-Verlag, Berlin, 1991).
[2] J. B. Flor and G. J. F. van Heijst, ''An experimental study of dipolar vortex structures in a stratified fluid,'' J. Fluid Mech. **279**, 101 (1994).
[3] J. H. G. M. van Geffen and G. J. F. van Heijst, ''Viscous evolution of 2D dipolar vortices,'' Fluid Dyn. Res. **22**, 191 (1998).
[4] B. Cantwell and N. Rott, ''The decay of a viscous vortex pair,'' Phys. Fluids **31**, 3213 (1988).
[5] D. W. Moore and P. G. Saffman, ''The instability of a straight vortex filament in a strain field,'' Proc. R. Soc. London, Ser. A **346**, 413 (1975).
[6] S. C. Crow, ''Stability theory for a pair of trailing vorticies,'' AIAA J. **8**, 2172 (1970).
[7] T. Leweke and C. H. K. Willliamson, ''Cooperative elliptic instability of a vortex pair,'' J. Fluid Mech. **360**, 85 (1998).
[8] P. Orlandi, G. F. Carnevale, S. K. Lele, and K. Shariff, ''DNS study of stability of trailing vortices,'' *Center for Turbulence Research*, Stanford Proceedings of the Summer Program 1998, pp. 187.
[9] D. duP. Donaldson and A. J. Bilanin, ''Vortex wakes of conventional aircraft,'' AGARD-AG-204, May 1975.
[10] H. Lamb, *Hydrodynamics* (Cambridge University Press, Cambridge, 1906).
[11] V. V. Meleshko and G. J. F. van Heijst, ''On Chaplygin's investigations of two-dimensional vortex structures in an inviscid fluid,'' J. Fluid Mech. **272**, 157 (1994).
[12] T. H. Lê, B. Troff, P. Sagaut, K. Dang-Tran, and T. P. Loc, ''PEGASE: a Navier–Stokes solver for direct numerical simulation of incompressible flows,'' Int. J. Numer. Methods Fluids **24**, 833 (1997).
[13] P. G. Saffman, *Vortex Dynamics* (Cambridge University Press, Cambridge, 1992).